Wavelet Transform-Based QRS Complex Detector

Shubha Kadambe,* *Member, IEEE*, Robin Murray, and G. Faye Boudreaux-Bartels

***Abstract*—In this paper, we describe a QRS complex detector based on the dyadic wavelet transform (D_yWT) which is robust to time-varying QRS complex morphology and to noise. We design a spline wavelet that is suitable for QRS detection. The scales of this wavelet are chosen based on the spectral characteristics of the electrocardiogram (ECG) signal. We illustrate the performance of the D_yWT-based QRS detector by considering problematic ECG signals from the American Heart Association (AHA) data base. Seventy hours of data was considered. We also compare the performance of D_yWT-based QRS detector with detectors based on Okada, Hamilton–Tompkins, and multiplication of the backward difference algorithms. From the comparison, results we observed that although no one algorithm exhibited superior performance in all situations, the D_yWT-based detector compared well with the standard techniques. For multiform premature ventricular contractions, bigeminy, and couplets tapes, the D_yWT-based detector exhibited excellent performance.**

***Index Terms*— American Heart Association (AHA) database, Dyadic wavelet transform (D_yWT) and its properties, performance comparison, QRS detector, robust detector.**

I. Introduction

THE detection of the QRS complex—specifically, the detection of the peak of the QRS complex, or R wave—in an electrocardiogram (ECG) signal is a difficult problem since it has a time-varying morphology and is subject to physiological variations due to the patient and to corruption due to noise. For a tutorial on ECG signals, readers are referred to [1]. Since the QRS complexes have a time-varying morphology, they are not always the strongest signal component in an ECG signal. Therefore, P-waves or T-waves with characteristics similar to that of the QRS complex, as well as spikes from high-frequency pacemakers can compromise the detection of the QRS complex. In addition, there are many sources of noise in a clinical environment that can degrade the ECG signal. These include power line interference, muscle contraction noise, poor electrode contact, patient movement, and baseline wandering due to respiration [2]. Therefore, QRS detectors must be invariant to different noise sources and should be able to detect QRS complexes even when the morphology of the ECG signal is varying with respect to time.

As noted in [3], most of the current QRS detectors can be divided into two stages: a preprocessor stage to emphasize the QRS complex and a decision stage to threshold the QRS enhanced signal. Typically, the preprocessor stage consists of both linear and nonlinear filtering of the ECG. The ECG signal is first bandpass filtered to reduce noise and differentiated to emphasize the large slope of the R wave; it is then squared to further exploit the high-frequency content of the QRS complex. A short-time energy estimate is obtained by smoothing the resulting signal with a moving window integration.

The selection of the bandwidth of the bandpass filter and the duration of the sliding analysis window is not always straightforward. The bandwidth of the bandpass filter must be chosen to reflect the tradeoff between noise reduction and loss of high-frequency details; if the bandwidth is too large, noise reduction suffers. If the bandwidth is too narrow, high-frequency QRS characteristics are lost. A short-time energy detector is developed using a sliding analysis window. The choice of the duration of the sliding window results in a tradeoff between false and missed detections. A long window allows a large energy accumulation which easily exceeds a threshold, whereas a narrow window duration allows too little energy to accumulate. In short, in the frequency domain, the fixed bandwidth of the bandpass filter cannot adapt to changes in the bandwidth of the QRS complex, and in the time domain, the fixed length of the moving window cannot adapt to changes in the duration of the QRS complex. Therefore, a disadvantage of a prefixed bandpass filter/short-time energy technique is that it does not accurately account for the inherent time-varying morphology of the QRS complex. That is, they do not adapt very well to changes in QRS morphology. To overcome the limitations imposed by fixed duration windowing techniques in detecting time-varying transients, a general, adaptive technique that captures the spectral/temporal variations in QRS morphology is needed. In this paper, one such technique based upon the dyadic wavelet transform (D_yWT) is proposed. A chosen "mother wavelet" has a fixed shape; however, the wavelet functions derived from it by changing scales, referred to as "daughter" wavelets, have different bandwidths and time supports. At any particular scale, the D_yWT is the convolution of the signal and a dyadically time-scaled daughter wavelet. Scaling the mother wavelet is the mechanism by which the D_yWT adapts to the spectral and temporal changes in the signal being analyzed. The D_yWT inherently has a multiresolution capability. For small scale values, it exhibits high temporal and low spectral resolution whereas for large scale values, it exhibits low temporal and high spectral resolution.

A multiresolution approach to signal analysis using the wavelet transform (WT) has been previously applied in many fields. For a tutorial on wavelet theory and applications, refer to [4], [6]. In [7] and [8], the D_yWT was applied for edge detection and image compression, while in [9] it was used to extract pitch period information from voiced

Manuscript received June 6, 1996; revised March 1, 1999. This work was supported in part by the U.S. Office of Naval Research (ONR) under Grant N00014-89-J-1812. *Asterisk indicates corresponding author.*

*S. Kadambe is with the Information Sciences Laboratory, HRL Laboratories, LLC, Malibu CA 90265 USA (e-mail: skadambe@hrl.com).

R. Murray and G. F. Boudreaux-Bartels are with the Department of Electrical Engineering, University of Rhode Island, Kingston, RI 02881 USA.

Publisher Item Identifier S 0018-9294(99)04699-6.

speech segments. The D_yWT has also been previously applied to ECG analysis in the context of 1) detecting ventricular late potentials (VLP's) [10], and 2) separating the various waves (P, R, and T) in the ECG [11]. In [11], the authors' concluded that the waveforms could not be distinguished using the D_yWT since their spectra overlapped. However, because the QRS complex is a transient, and because the D_yWT computed using a special wavelet exhibits local peaks across several scales at the instance of occurrence of transients, it is reasonable to assume that QRS complexes could be detected by tracking peaks in its D_yWT across successive dyadic scales. Since our initial study on applying the D_yWT to QRS detection [12] in 1992, researchers in China [13] have independently applied the D_yWT for detecting the QRS complex in 1993. Subsequently, a more detailed paper by the same authors is published [14]. It should be noted that in their algorithm they compute the D_yWT for *a priori* fixed four scales. However, in our approach a specific spline wavelet, suitable for the analysis of QRS complexes, is designed and the scales are chosen adaptively based on the signal. We compute the D_yWT at two consecutive scales and if necessary, compute the D_yWT at one additional scale. Usually, we only need to compute the D_yWT at two scales which has a computational advantage as compared to [14]. Further, in [14] the authors have tested their algorithm on the MIT/BIH database, whereas our algorithm was tested on the AHA database. In addition, we have exhaustively compared the performance of our algorithm with other standard techniques using the same database. Similar to authors in [13], [14], we have also observed that the D_yWT-based QRS detector is robust to noise. Even though, the authors in [13] and [14] have shown that it is possible to apply their algorithm to detect other waves such as P, T, etc., in this paper, we have primarily concentrated on detecting R waves since we are interested in estimating the heart rate.

In this paper, a QRS detector based on the D_yWT is described that is robust both to noise and to time-varying morphologies in the QRS complex. In Section II, a brief review of the WT, including relevant properties, is provided. Specifically, we focus on the transient detection capability of the D_yWT and its relation to the QRS detection problem. In Section III, the D_yWT-based QRS detector is compared with previously developed QRS detection schemes. In Section IV, the D_yWT-based QRS detector is evaluated using the AHA database.

II. A Brief Review of the Wavelet Transform

The continuous wavelet transform (CWT) of a signal $x(t)$ is defined as [15], [16]

$$\mathrm{CWT}_x(b,a) = \frac{1}{\sqrt{|a|}} \int_{-\infty}^{\infty} x(t) g^*\left(\frac{t-b}{a}\right) dt \qquad (1)$$

where the wavelet function, $g(t)$, satisfies the admissibility conditions mentioned in [16], and b and a ($b, a \in \Re$, and $a \neq 0$) are the translation and dilation parameters, respectively. The duration of the mother wavelet $g(t)$ is either compressed or expanded depending upon the choice of a. Hence, the CWT can extract both local and global variations of a signal $x(t)$. The CWT can also be considered as the output of a bank of bandpass filters whose center frequencies and bandwidths vary depending on the dilation parameter a in addition to the spectral properties of the wavelet function.[1] The variable bandwidth introduces different resolutions at different scales and thus, the CWT has a multiresolution capability. If the signal $x(t)$ or one of its derivatives have discontinuities, then the modulus of the CWT of $x(t)$, $|\mathrm{CWT}_x(b,a)|$, exhibits local maxima around the time of occurrence of the discontinuities and the lines of constant phase of the $\mathrm{CWT}_x(b,a)$ converge toward the point of discontinuities.[2] Thus, the CWT exhibits the property of "zooming" in on the sharp temporal variations in a signal.

The main disadvantages of the CWT are computational complexity and redundancy. However, they can be reduced by discretizing either a or by discretizing both a and b. The CWT is defined as the dyadic wavelet transform (D_yWT), if only a is discretized along the dyadic sequence 2^i where $i = 1, 2, \cdots$. The D_yWT of a signal $x(t)$ is then defined as [7]

$$D_y\mathrm{WT}_x(b,2^i) = \frac{1}{\sqrt{2^i}} \int_{-\infty}^{\infty} x(t) g^*\left(\frac{t-b}{2^i}\right) dt. \qquad (2)$$

In the case of the D_yWT, the wavelet function $g(t)$ should satisfy the additional constraint $\Sigma_{i=-\infty}^{\infty} |G(2^i\omega)|^2 = 1$ where $G(\omega)$ is the Fourier transform (FT) of $g(t)$. This condition ensures that the whole frequency axis is covered by dilations of $G(\omega)$ by the scale factors 2^i. Due to the dyadic sampling of the scale parameter, the D_yWT can be considered as the output of a bank of *octave* band filters. The advantages of the D_yWT are (1) reduction in computational complexity and redundancy of the CWT and (2) maintenance of most of the nice properties of the CWT such as linearity, shift covariance, scale covariance, and the "zooming property".

In [7], it was shown that if the wavelet is chosen as the first derivative of a smoothing function (a function whose FT has energy concentrated at low frequencies) then the local maxima of the absolute value of the D_yWT indicate the occurrence of sharp signal variations while the local minima indicate the occurrence of slow signal variations, provided the first and second derivatives of the smoothing function exist. Furthermore, it was shown in [7] that sharp changes in a signal at time $t = t_0$ exhibit local maxima in the $|D_y\mathrm{WT}|$ at time $t = t_0$ across.

Since the D_yWT computed using a wavelet which is the first derivative of a smoothing function exhibits local maxima at several successive scales at the time of occurrence of transients, and since the QRS complex is a transient in the ECG signal, we propose using the D_yWT to detect the QRS complex. Indeed, this property of alignment of local maxima of the D_yWT has been successfully used for 1) edge detection and image compression in [7], [8], and 2) pitch detection

[1] An important distinction exists between a mother wavelet and an arbitrary bandpass filter: a mother wavelet is regular, whereas a bandpass filter, in general, is not regular [6].

[2] A wavelet function, $g(t)$, with n vanishing moments, $\int t^m g(t)\, dt = 0,\ (m < n)$ is necessary to identify singularities with Lipschitz exponents up to a value of n.

and estimation of the pitch period in speech signals in [9]. Perturbations in the local maxima are accounted by applying a pruning technique that is described in Section III-A.

III. QRS Detection

In this section, we describe the D_yWT-based QRS detector and review some of the QRS detectors which we have used for the comparison of the performance of the D_yWT-based QRS detector in Section IV.

A. The D_yWT-based QRS Detector

The algorithm of the D_yWT-based QRS detector is as follows:

- Compute the D_yWT of a *windowed* portion of length L_w seconds of an ECG signal at the dyadic scales $a = 2^i, i = i_m, i_{m+1}, \cdots, i_u$. In this study, L_w was set to 2.05 s (512 samples). The starting index i_m and the ending index i_u are chosen based upon known physical constraints which will be explained later. Here, similar to [7], [8] and to [9], we detect QRS complexes by making use of the property that the absolute value of D_yWT has localized maxima across several consecutive scales at the instant of the occurrence of transients. For each scale 2^i, we locate the local maxima of the absolute value of $D_y\mathrm{WT}(b, 2^i)$ which exceed a given local threshold. In this study, we empirically found that a choice of 60% as the `local` threshold value (i.e., 60% of the maximum value of the $|D_y\mathrm{WT}|$ in each windowed portion of data) gave the best results. Hence, in all the examples of the simulation section, we use 0.6 as the local threshold value. We consider both the number and the locations of thresholded local maxima (peaks) of the $|D_y\mathrm{WT}|$ at the scale, $a = 2^i$ and at the scale $a = 2^{i+1}$. If the number of peaks is the same, and the location of the peaks align within ± 25 samples (± 0.1 s)[3] neighborhood of time across two consecutive scales, we assume that the locations of these maxima correspond to the location of possible QRS complexes. However, if the number of peaks agrees but the locations exceed ± 25 samples time neighborhood, the thresholded data is pruned of the offending misaligned peaks. The locations of peaks that align across the two consecutive scales are stored in a vector of possible QRS complexes. If the number of peaks does not agree across two consecutive scales, the D_yWT is computed at the next dyadic scale, and the procedure described above is repeated while $i \leq i_u$.

  Next, the vector of possible QRS complexes is searched for refractory peaks. Any peak in the vector of possible QRS complexes occurring within a refractory period (0.2 s or 50 samples)[4] of a previously thresholded peak is disregarded since the refractory period represents the interval immediately following a QRS complex during which no further excitation of the cardiac tissue can initiate another QRS complex. Thus, detection of false peaks can be minimized, and the locations represent the time of occurrence of the transient R waves. We then estimate the heart rate by computing the inverse of the time interval between two consecutive R waves.
- The D_yWT is generally computed at scales 2^i for, theoretically, all i. However, we can restrict the range of scale parameters needed to compute the D_yWT based on the nature of the signal under study. Using the procedure outlined in [9], we designed a cubic spline mother wavelet with center frequency equal to 120 Hz and a bandwidth of 240 Hz. Since the average spectral support of the QRS complexes is 6–30 Hz and most of the spectral power of motion artifact and muscle noise is within 0–5 Hz as shown in [17], we chose the scales such that they cover the spectral support of QRS complexes. Such a selection of scales helps in filtering out noise. Consequently, the algorithm starts with the scale, 2^{i_m} (index $i_m = 1$), corresponding to center frequency of 60 Hz and bandwidth 120 Hz, and continues up to a maximum scale, 2^{i_u} (index $i_u = 3$), corresponding to center frequency of 15 Hz and bandwidth of 30 Hz. This is the upper limit. The algorithm *does not* compute the D_yWT beyond this scale. If the algorithm fails to find any matching peaks at this scale, then it declares that there are no QRS complexes in the data segment and proceeds to the next data segment. After choosing the lowest and highest scales, we compute the D_yWT at the lowest scale and double the scale parameter (if the number of peaks and their locations do not match at two successive scales) until the highest scale is reached. To better understand this point, refer to Fig. 2. In Fig. 2(a), a noisy ECG signal segment of length 500 samples is plotted. In Fig. 2(b), the magnitude of D_yWT computed at the smallest scale i.e., $i = 1$ is plotted with the peak locations estimated by the algorithm. In Fig. 2(c), the magnitude of D_yWT at the next scale is plotted with peak locations. From Fig. 2(b) and (c), it can be seen that the number of peaks and their locations do not match because at the lower scale the noise is not completely filtered out and there are more false peaks (false alarms) corresponding to transients in noise. In Fig. 2(d), the magnitude of D_yWT at upper limit $i = 3$ is plotted. By comparing Fig. 2(c) and (d) it can be seen that the number of peaks and peak locations match at these two scales. At this point the algorithm declares that there are QRS complexes present in the segment and estimates their locations as the location of the peaks. The algorithm then estimates the heart rate as the inverse of the time interval between two consecutive peaks. In case the number of peaks and their locations at scale $i = 3$ did not match with scale $i = 2$, the algorithm would have concluded that this segment does not have QRS complexes and would continue to analyze the next segment. Thus we compute the D_yWT at most at three scales $2^1, 2^2$, and 2^3, which significantly reduces computational complexity. Since computing the D_yWT at any one scale is independent of computing the D_yWT at any other scale, the computation can be performed simul-

[3] We allow a misalignment of ± 25 samples across two consecutive scales since a valid QRS complex cannot occur within the refractory period (0.2 s) and, hence, the misaligned peaks should correspond to the same QRS complex.

[4] The ECG data from the AHA database is sampled at 250 (samples/s).

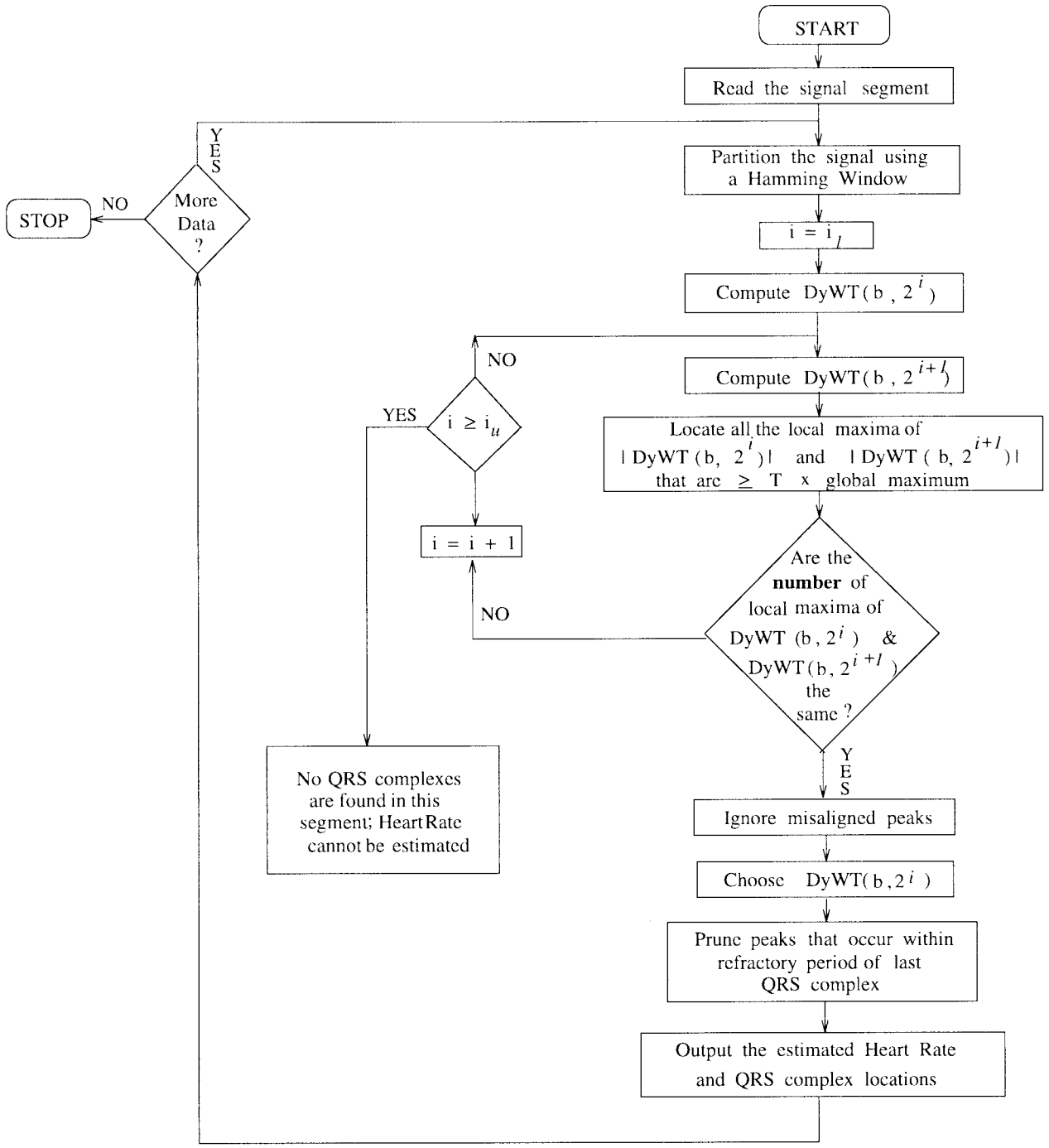

Fig. 1. Flow chart of the D_yWT-based QRS detector.

taneously. This may enable the real time implementation of the D_yWT-based QRS detector. However, the use of fast decomposition algorithms is precluded due to the choice of overlapping (nonorthogonal) wavelet functions.

The flow chart of the algorithm is shown in Fig. 1. We compare the performance of the D_yWT QRS detector with QRS detectors developed by Okada [18], Suppappola and Sun [19], and Hamilton and Tompkins [20], that are implemented from the respective papers in [19]. For the sake of completeness, these algorithms are briefly described in the following three sections. Note that the performance comparison is only with respect to detection accuracy. Even though it is possible to achieve real time implementation of the D_yWT QRS detector, we are not concentrating on real time detection capabilities of the QRS detectors in this paper.

B. Okada Algorithm

The Okada algorithm [18] is an early application of digital filtering techniques to the problem of QRS detection. The difference between 1) a three-point moving average of the ECG signal and 2) a more severe low-pass filtering of the ECG is computed, which effectively produces a bandpass

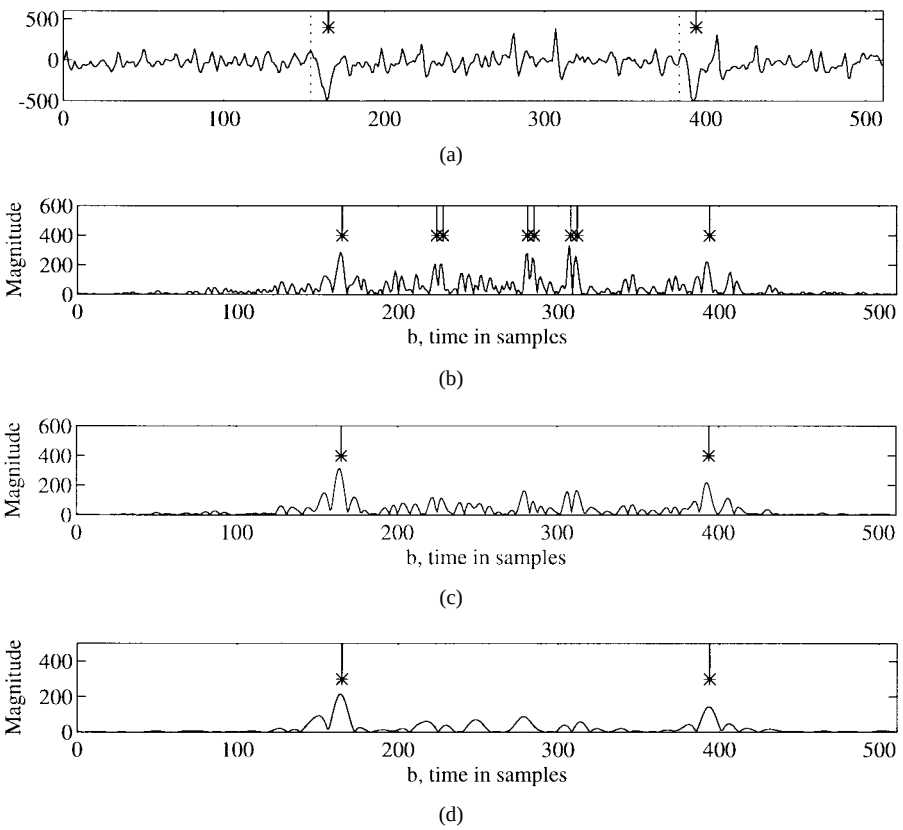

Fig. 2. Tape 3203 [isolated multiform premature ventricular contractions (PVC's)]: (a) noisy portion of ECG data plotted with vertical dashed lines indicating cardiologist estimate of the QRS onset and with tic marks indicating the D_yWT estimate of the R wave locations. (b)–(d) $|D_yWT(b, 2^i)|$ computed at $a = 2^1, 2^2$, and 2^3, respectively. Note, the number of peaks and their locations align at scales $a = 2^2$, and $a = 2^3$.

filtering operation on the original data. The difference signal is then squared. To further highlight the high-frequency QRS complex, the resulting signal is multiplied by a nonlinearly filtered version of itself. False peaks in the resulting signal occurring due to abrupt baseline wandering are removed by searching the output of the 3 point moving average filter for local peaks.

C. MOBD Algorithm

The class of algorithms proposed by Suppappola and Sun [19], referred to as multiplication of the backward difference (MOBD), use only nonlinear filtering to detect the QRS complex. The traditional preprocessing of the ECG signal with linear filtering techniques is omitted, thus permitting a faster detector response time. Moreover, the detector quantizes the ECG signal to a fewer number of bits before applying the nonlinear MOBD transformation. In effect, the quantizer de-emphasizes the small amplitude, low-frequency P and T waves, while simultaneously emphasizing the large amplitude, high-frequency QRS complexes.

A typically employed technique to emphasize the high-frequency characteristics of a signal is to square the "derivative" (or backward difference) of the signal. However, signals that are characterized by both a large amplitude and by a large slope, such as the QRS complex, can be further exploited by multiplying together multiple *successive* samples of the backward difference of the signal. In addition, increasing the quantization of the ECG signal actually improves the detector's performance. Since many successive samples of the backward difference of the ECG signal are multiplied together, the de-emphasized signal components which do not have sufficient amplitude and high-frequency content (such as the P and T waves) will result in a zero magnitude backward difference when the MOBD transformation is applied.

D. Hamilton–Tompkins Algorithm

The QRS detector developed by Hamilton and Tompkins uses a bandpass filter-based preprocessor [21] with an optimized decision stage for QRS detection. The preprocessor employs both linear and nonlinear filtering of the ECG to exploit the slope, duration, and amplitude information of the QRS complex. A digital bandpass filter restricts the frequency passband from 5–12 Hz to reduce noise effects. Next, the large slope of the R wave is enhanced by differentiating and then squaring the signal. The resulting signal is then smoothed using a moving window integration to obtain a short-time energy estimate which is then used as a detection statistic.

It should be noted that the proposed D_yWT algorithm is conceptually similar to the Hamilton–Tompkins algorithm in that both techniques effectively bandpass filter and differentiate the ECG signal. However, there are two significant advantages of the proposed D_yWT QRS detector: 1) since the octave bandpass filters of the D_yWT are scaled versions of one another, the D_yWT QRS detector can adapt to changes

in the bandwidth of the QRS complex and 2) unlike regular bandpass filtering, the D_yWT has the additional property that if a wavelet which is the first derivative of a smoothing function is used, peaks of the D_yWT correlate across successive dyadic scales at the occurrence of a transient.

IV. Illustrative Examples

In the following examples, specific examples of applying each algorithm to the entire[5] AHA database are given. The results for the other AHA database tapes that are not mentioned below can be found in [19] and [22]. The AHA database consists of 80 dual channel ECG data tapes providing more than 40 hours of data. Cardiologist have manually identified the time of occurrence and classified the type of QRS complex anomaly for each tape. The time of occurrence of each QRS complex is consistently marked at the onset of the R wave (near the Q wave). Although both channels of the same tape have the same cardiologist annotations, this information was not used to improve the detection of QRS complexes in the other channel. Each channel of ECG data was analyzed independently. Each series of ten tapes (e.g., tapes 2201–2210) is classified according to a particular ECG anomaly (e.g., isolated uniform PVC's. The last series of tapes (tapes 8201–8210) are characterized by ventricular fibrillation/flutter—a state in which the heart is not beating. The performance in this series of tapes is not included here because for large portions of each tape, there are no QRS complexes to detect.

In the case of the D_yWT-based QRS detector, the analysis is performed on a frame by frame basis until the end of the data is reached. Each frame is of length L_w and is obtained by using a Hamming window of length $L_w = 2.05$ s. Subsequent frames of the data are obtained by overlapping the window by 75%. In the case of the analysis of the first frame, the algorithm may experience start up detection errors due to the following reasons: 1) usage of a noncausal window and 2) the truncation of the data which fall within the tail of the Hamming window. However, in the case of the subsequent frames, we can overcome the start up errors by overlapping the window.

In the first two examples, we demonstrate that the D_yWT-based QRS detector is robust to noise. In the first example, the ECG is corrupted with external noise (tape 3203) and in the second example the ECG exhibits baseline wandering (tape 1209). The subsequent examples show the detector's performance to two different arrhythmias. Tape 2206 exhibits PVC's. PVC's are QRS complexes that do not arise along the normal conduction route. Tape 4205 exhibits bigeminy, a rhythm which alternates between a fast and a slow rate. For visual clarity, only a portion (900 samples) of each tape from the AHA database is plotted in Fig. 3(a)–(c), respectively.

A. AHA Tape 3203

In Fig. 2(a), the noise corrupted ECG signal is plotted along with the cardiologists annotation i.e., fiducial markings, (vertical dashed line) of the QRS complex onset and the D_yWT estimate of the QRS location (tick mark at the top of the diagram). A delay between the two marks occurs because the cardiologist's annotation mark identifies the onset of the QRS complex (near the Q wave) whereas, the D_yWT typically tracks the peak of the QRS complex (R wave).

The three subsequent figures show the $|D_y\mathrm{WT}(b, 2^i)|$ computed at the scales $a = 2^1, 2^2$, and 2^3, respectively. Tic marks indicate where the local maxima exceed the threshold which is chosen as 60% of the maximum peak at that scale. At the scale $a = 2^1$, eight peaks exceed the threshold [Fig. 2(b)], and at the subsequent scale $a = 2^2$, two peaks exceed the threshold [Fig. 2(c)]. Since the number of local maxima do not agree across the first two successive scales, the algorithm computed the D_yWT at the next dyadic scale $a = 2^3$, [Fig. 2(d)]. In this case, the local maxima at the scales $a = 2^2$ and 2^3 agree in number and in location; the location of these local maxima correspond to the D_yWT algorithm's estimate of the location of the R waves.

The accuracy of each technique for the noise corrupted ECG signal is given in Table I, where the performance criterion is the percentage of error rate (error rate $= (FP + FN/\text{total number of beats})$), where FP denotes the number of false positives and corresponds to a detector error of detecting a QRS complex where there is none and FN denotes the number of false negatives (FN's) and corresponds to a detector error of not detecting a QRS where there is one, respectively. An estimated QRS complex is classified as a valid detection, a FN, or a FP based on the cardiologist annotation marks since they define what is and what is not a QRS complex location. For this example, the D_yWT detector exhibits the best performance with an error rate of 2.6%. The noise sensitivity of the Okada algorithm is reflected in the large number of FP's, yielding an error rate of 34.2%.

B. AHA Tape 1209

In this example [Fig. 3(a)] the ECG signal exhibits baseline wandering which makes it appear to be superimposed on a low-frequency oscillation. Because the wavelet function $g(t)$ is a bandpass (zero mean) function, it can remove constant baseline drift, but not the low-frequency oscillation. The D_yWT's performance for the entire tape 1209 is given in Table I and is better than that of the conventional methods.

C. AHA Tape 2206

QRS detectors should be able to detect a wide variety of abnormal QRS complexes. One such anomaly is a PVC, which is distinguished from a normal heart beat by its early occurrence (resulting in an irregular heart rate) and longer duration. A portion of ECG data including a PVC (second QRS complex near sample number 200) is shown in Fig. 3(b). All four techniques identify the normal QRS complexes and the PVC without error. The excellent performance of all four detectors for Tape 2206 is given in Table I.

D. AHA Tape 4205

In Fig. 3(c), a portion of the ECG signal reflects a time-varying cardiac arrhythmia known as bigeminy. Identifying bigeminy is difficult since one of the QRS complexes has a small amplitude. In addition, the magnitude of the QRS

[5] excluding the ventricular fibrillation/flutter tape series.

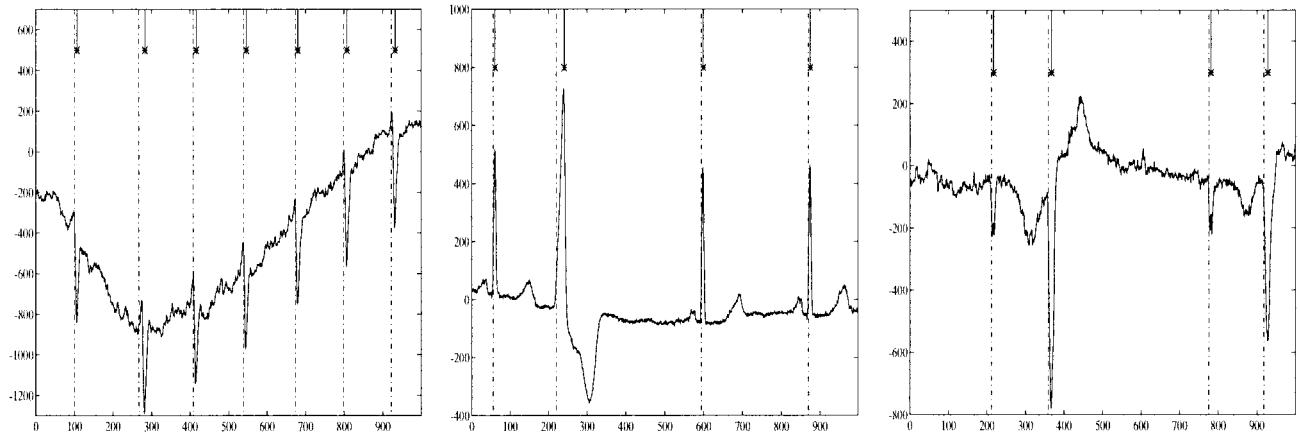

(a) (b) (c)

Fig. 3. ECG data from AHA Tapes 1209 (a), 2206 (b), 4205 (c). In (a)–(c), vertical dashed lines indicate the cardiologists' estimate of the QRS onset and tic marks indicate the D_yWT estimate of the R wave locations. The horizontal axis is time in units of samples (a) contains ECG data from tape 1209 (no PVC's) which is corrupted by baseline wander. Tape 2206 in (b) contains a portion of ECG data exhibiting an isolated uniform PVC, and (c) contains a portion of ECG data from tape 4205 exhibiting bigeminy.

TABLE I
A COMPARISON OF THE PERFORMANCE OF THE QRS DETECTION CAPABILITY OF THE FOUR ALGORITHMS ON CHANNEL 1 OF THE ENTIRE 30 min OF AHA TAPES 3203 (ISOLATED MULTIFORM PVC'S), 1209 (NO PVC'S), 2206 (SINGLE UNIFORM PVC'S) AND 4205 (BIGEMINY)

Tape #	Algorithms on channel 1 - 30 min											
	# beats	D_yWT			H–T			MOBD			Okada		
		FP	FN	% error	FP	FN	% error	FP	FN	% error	FP	FN	% error
3203	1950	40	11	2.6	86	22	5.6	259	40	15.4	610	54	34.2
1209	3583	157	258	11.6	46	1114	32.6	6	1339	37.7	21	1341	38.2
2206	1613	2	1	0.2	1	0	0.1	0	0	0.0	0	21	1.3
4205	1452	221	2	15.4	61	71	9.1	28	57	5.0	11	165	12.2

complexes comprising the bigeminy also varies. The results for a specific case of tape 4205 are given in Table I. For this particular tape, the MOBD exhibited the minimum error rate of 5%, whereas the D_yWT had the highest error rate of 15.4%. It is interesting to note, that the D_yWT had a minimum number of FN's (only two) in comparison to the MOBD which had 57 FN's. However, for the whole 4200 tape series which included bigeminy, the D_yWT exhibited the lowest error rate using a 1% error rate criterion, see Table III. This indicates the robustness of D_yWT.

Note that in all the above mentioned cases. the D_yWT has the least number of FN's (see Table I) indicating that it did not miss as many QRS complexes as other algorithms did. In many situations false alarms are more tolerated than missing the detection of QRS complexes. The results of Table I indicates that by further optimizing the threshold and peak pruning, the performance of the D_yWT can be improved by reducing the false alarm or FP.

V. OVERALL PERFORMANCE

In the previous section, illustrative examples were given to understand the cases under which the D_yWT algorithm performs better or worse. However, the true performance of an algorithm can only be measured when it is tested on a large database. Hence, in this section we consider 70 h of AHA data. Due to the inordinate amount of data generated in comparing the error rates of all four algorithms on 70 dual channel tapes, corresponding to about 70 h of data from the AHA database, listing the results in tabular form was precluded since it was both an inefficient and obscuring manner in which to present the results. Thus, the interested reader is directed to [22] for tables comparing the error rates for all four algorithms on the AHA database.

QRS detectors should perform well even in the presence of noise. Here, we consider two noise artifacts: electromyographic (EMG) noise due to muscle contraction and 60-Hz power-line interference. In these two examples, the results are for the D_yWT detector on the small noisy portions of data are shown. To examine the effects of EMG interference, we simulated this type of noise according to [2], and added it to ECG data from the AHA database. The simulated muscle contraction noise is modeled as a zero-mean, 10-KHz bandwidth Gaussian random signal, with standard deviation equal to 10% of the peak-to-peak ECG amplitude. The original ECG data (250-Hz sampling rate), along with the cardiologist's annotation marks and the results of the D_yWT detector are shown in Fig. 4. The ECG signal corrupted by the simulated muscle contraction noise (20 KHz sampling rate) is shown in Fig. 4(b). Since ECG data from the AHA database is sampled at 250 Hz, we next downsampled the signal in Fig. 4(b) to

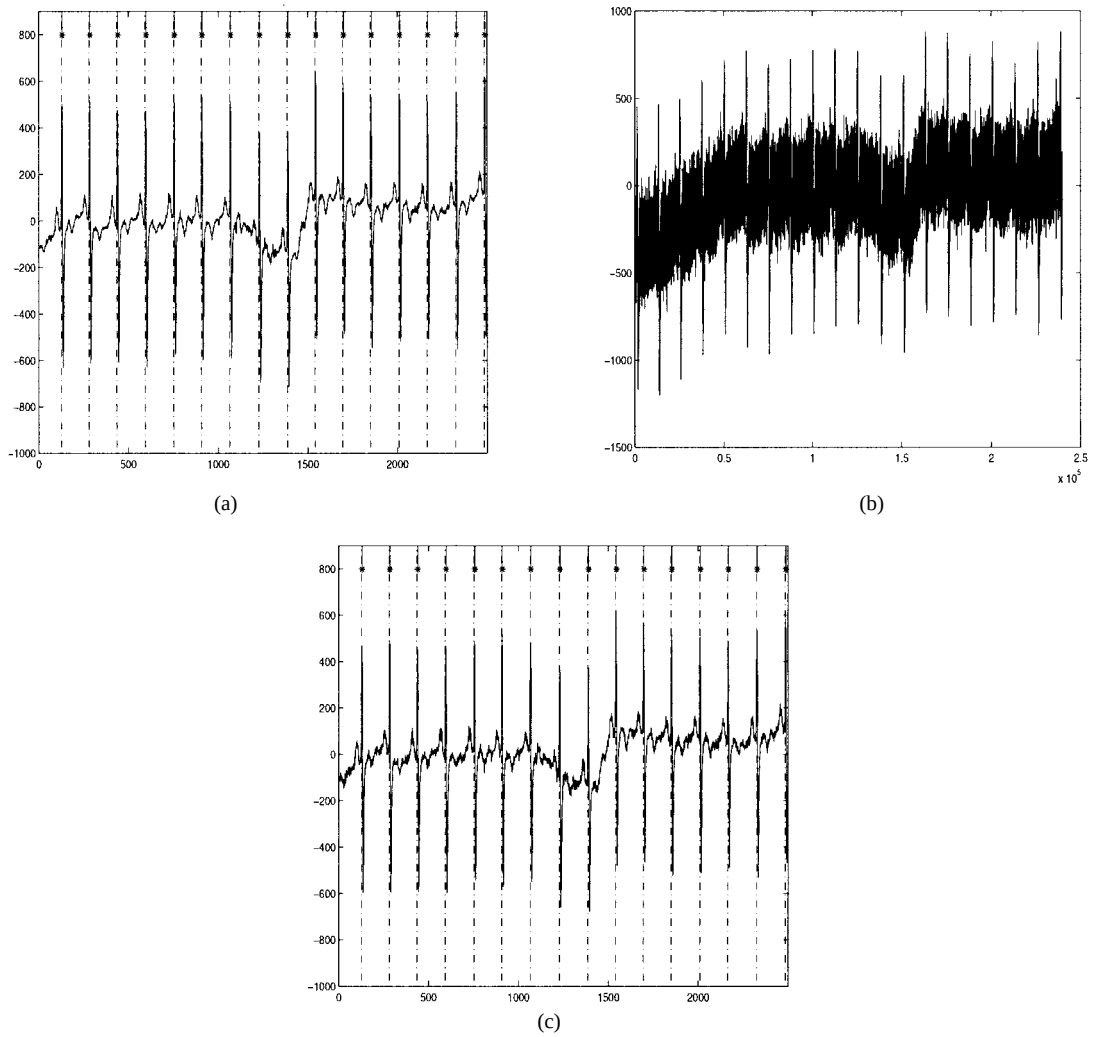

Fig. 4. ECG data from AHA Tape 1204 (250-Hz sampling rate) plotted with vertical dashed lines indicating cardiologist estimate of the QRS onset and with tic marks indicating the D_yWT estimate of the R wave locations is shown in (a). The horizontal axis is time in units of samples. (b) and (c) show the ECG data in (a) corrupted by simulated muscle contraction noise at a 20 KHz. sampling rate, and downsampled to the 250-Hz. sampling rate of the AHA database, respectively.

obtain a 250-Hz sampling rate. The results of the D_yWT on the downsampled signal are shown in Fig. 4(c). Although the original, uncorrupted ECG signal and the downsampled, muscle noise corrupted signal differ, the QRS locations from the D_yWT QRS detector for the noisy data differ from the original uncorrupted data at most by only one sample.

The next source of noise that we examine is 60-Hz noise. 60-Hz powerline interference is a typical source of noise corruption for the ECG signal. A portion of ECG data exhibiting 60-Hz interference in Fig. 5 shows that the D_yWT detector accurately identifies the R waves.

In Figs. 6–8, we summarize the performance of the D_yWT QRS detector with each algorithm on channel 1 of the ECG data from 70 tapes from the AHA database. To facilitate the comparison of the D_yWT-based QRS detector's performance against the other three algorithms, the tapes were sorted such that the D_yWT error rate appears in nondecreasing order, along with the associated error rate of the other algorithm (Hamilton–Tompkins, MOBD, or Okada) for that particular tape. Error rates greater than 40% were not displayed. Since the D_yWT error curve remains the same, this permits a fair and easy comparison between the three figures. Since the actual four digit tape numbers, which no longer (necessarily) occur

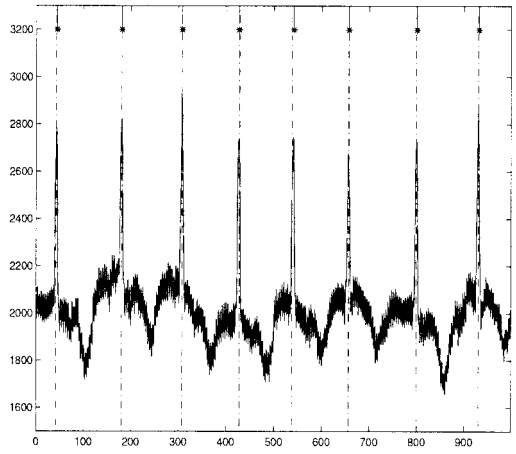

Fig. 5. Tape 8210 (60-Hz noise): A portion of ECG data corrupted by 60-Hz powerline noise plotted with vertical dashed lines indicating cardiologist estimate of the QRS onset and with tic marks indicating the D_yWT estimate of the R wave locations.

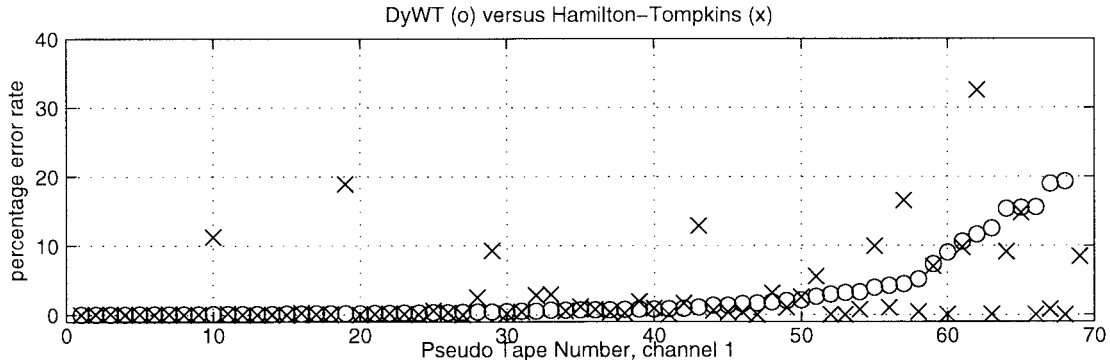

Fig. 6. Channel 1: Comparison of the percentage error rate for the D_yWT QRS detector versus the Hamilton–Tompkins algorithm. The tapes are sorted in order of nondecreasing error rate for the D_yWT.

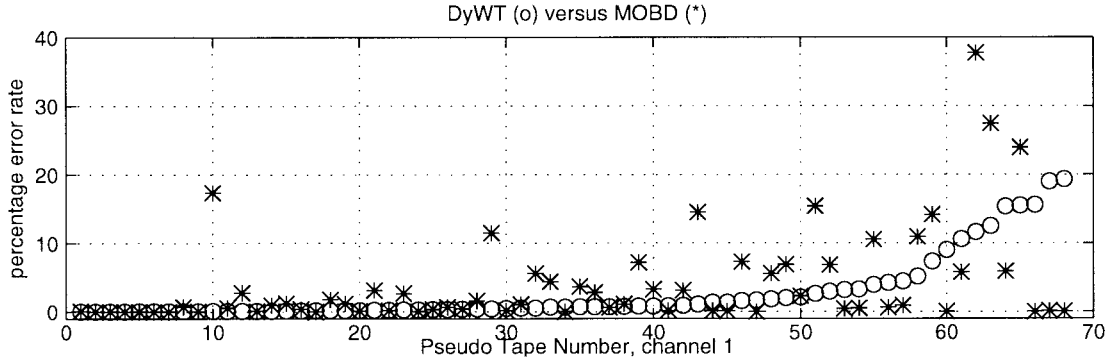

Fig. 7. Channel 1: Comparison of the percentage error rate for the D_yWT QRS detector versus the MOBD QRS detector algorithm. The tapes are sorted in order of nondecreasing error rate for the D_yWT.

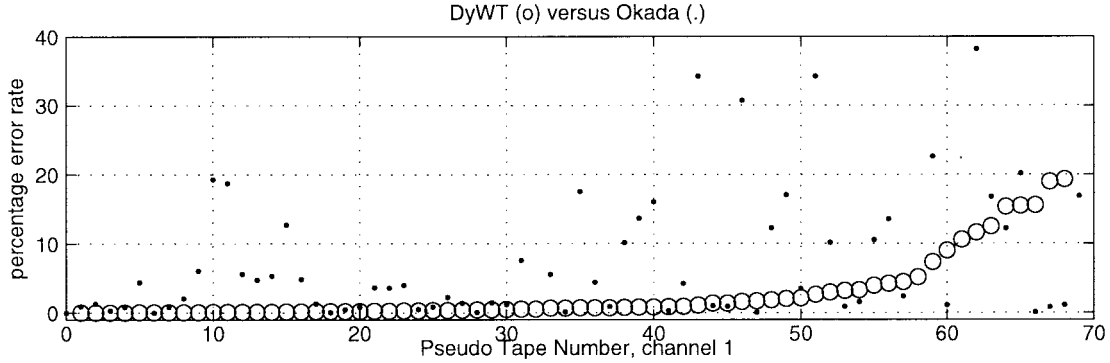

Fig. 8. Channel 1: Comparison of the percentage error rate for the D_yWT QRS detector versus the Okada QRS detector algorithm. The tapes are sorted in order of nondecreasing error rate for the D_yWT.

sequentially, could not be displayed along the horizontal axis, a sequential pseudotape number was assigned.

Table II compares the percentage of tapes in the AHA database, for each algorithm, that have an overall error rate of less than 1% and 5%, respectively. Using a 1% maximum error criterion, for channel 1, the Hamilton–Tompkins algorithm exhibits the best performance (66% of the tapes are within the 1% error criterion while the Okada algorithm exhibits the worst performance (only 27% of the tapes have an error rate of less than 1%). Note that when the error criteria is relaxed (less than 5%) the D_yWT-based QRS detector performs slightly better than the H-T method (for channel 1). Table III gives

TABLE II
PERCENTAGE OF TAPES FOR EACH ALGORITHM THAT HAVE ERROR RATES LESS THAN 1% AND 5%, RESPECTIVELY, FOR BOTH CHANNELS OF THE AHA DATABASE

Algorithm	< 1% error		< 5% error	
	channel			
	0	1	0	1
D_yWT	67.1	60.0	87.1	81.4
H–T	84.1	65.7	92.8	80.0
MOBD	60.9	50.0	85.5	71.4
Okada	42.0	27.1	68.1	57.1

TABLE III
PERFORMANCE OF EACH ALGORITHM ON A PARTICULAR ARRHYTHMIA, USING A 1% MAXIMUM ERROR

algorithm	Percentage of tapes with less than a 1% error						
	Tape series						
	1200's	2200's	3200's	4200's	5200's	6200's	7200's
D_yWT	50	80	70	60	50	40	70
H–T	70	90	70	50	60	40	80
MOBD	70	70	50	40	40	20	60
Okada	60	30	30	10	40	10	10

Ten 30–min tapes were analyzed in each series. The 1200's series contain no PVC's, the 2200's contain single uniform PVC's, the 3200's contain isolated multiform PVC's, the 4200's reflect bigeminy, the 5200's contain R on T beats, the 6200's contain couplets, and the 7200's contain ventricular rhythms.

a performance breakdown of each algorithm on a particular ECG abnormality for channel 1 using the 1% error criterion. From this table it can be seen that both D_yWT and the H-T method exhibited similar performance in most cases when a 1% error criterion was used.

VI. CONCLUSIONS

In this paper, a QRS detection algorithm based on the D_yWT was proposed. We have described the properties of the D_yWT necessary for ECG signal processing. We exploited the property that the onset of the local maxima of the $|D_y WT|$ of a transient signal correlates across successive dyadic scales if the mother wavelet is chosen as the first derivative of a smoothing function. The performance of the D_yWT-based detector was exhaustively examined by testing the algorithm on 70 h of data standardized AHA database. Moreover, these results were compared to those of well-known QRS detection algorithms. Although no one algorithm exhibited superior performance in all situations, the D_yWT-based QRS detector compared well with the standard techniques. In addition, in all the cases presented in the simulation section, the D_yWT has the least number of FN's indicating that it did not miss as many QRS complexes as other algorithms did. This indicates that by further optimizing the threshold and peak pruning, the performance of the D_yWT can be improved. Moreover, for multiform PVC's (3200 tape series), bigeminy (4200 series), and couplets (6200 series), (see Table III) tapes the D_yWT exhibited excellent performance. Thus, the primary advantages of the D_yWT over existing techniques are 1) its robust noise performance (external noise bursts found in the "multiform PVC" tape series, 60-Hz noise and simulated muscle noise) and 2) its flexibility in analyzing the time-varying morphology of ECG data (found in the bigeminy tape series and the couplet tape series). In this study, we used a fixed local threshold and did not optimize further the peak location selection. We expect that the D_yWT detector would perform better if the threshold and peak pruning techniques are optimized for the aforementioned reasons. Future work warrants the use of adaptive thresholding and adaptive peak pruning to improve the performance.

REFERENCES

[1] M. Armstrong, *Electrocardiograms*. Bristol, U.K.: Wright, 1985.
[2] G. M. Friesen, T. C. Jannett, M. A. Jadallah, S. L. Yates, S. R. Quint, and H. R. Nagle, "A comparison of the noise sensitivity of nine QRS detection algorithms," *IEEE Trans. Biomed. Eng.*, vol. 37, pp. 85–98, Jan. 1990.
[3] O. Pahlm and L. Sornmo, "Software QRS detection in ambulatory monitoring—A review," *Med. Biol. Eng. Comput.*, vol. 22, pp. 289–297, 1984.
[4] F. Hlawatsch and G. F. Boudreaux-Bartels, "Linear and quadratic time-frequency signal representations," *IEEE Signal Processing Mag.*, Apr. 1992, pp. 21–67.
[5] L. G. Weiss, "Wavelets and wideband correlation processing," *IEEE Signal Processing Mag.*, Jan. 1994, pp. 13–32.
[6] O. Rioul and M. Vetterli, "Wavelets and Signal Processing," *IEEE Signal Processing Mag.*, Oct. 1991, pp. 14–38.
[7] S. G. Mallat and S. Zhong, "Characterization of signals from multi-scale edges," *IEEE Trans. on Pattern Anal. Machine Intell.*, vol. 14, pp. 710–732, July 1992.
[8] S. Zhong and S. G. Mallat, "Compact image representation from multi-scale edges," presented at 3rd Int. Conf. on Comput. Vision, 1990.
[9] S. Kadambe and G. F. Boudreaux-Bartels, "Application of the wavelet transform for pitch detection of speech signals," *IEEE Trans. Inform. Theory*, vol. 38, no. 2, pp. 917–924, Mar. 1992.
[10] F. Tuteur, "Wavelet transformations in signal detection," in *Proc. IEEE Int. Conf. Acoust., Speech, Signal Processing*, New York, 1988, pp. 1435–1438.
[11] L. Senhadji, J. Bellanger, G. Carrault, and J. Coatrieux, "Wavelet analysis of ECG signals," in *Proc. Annu. Int. Conf. IEEE EMBS*, vol. 12, pp. 811–812, 1990.
[12] S. Kadambe, R. Murray, and G. F. Boudreaux-Bartels, "The dyadic wavelet transform-based QRS detector," *Proc. 26th Asil. Conf. Signal Systems Comput.*, Pacific Grove, CA, 1992, pp. 130–134.
[13] C. Li and C. Zheng, "QRS detection by wavelet transform," *Proc. 15th Ann. Int. Conf. IEEE Eng. Med. Biol. Soc.*, 1993, pp. 330–331.
[14] ——, "Detection of ECG characteristic points using wavelet transforms," *IEEE Trans. Biomed. Eng.*, vol. 42, pp. 21–28, Jan. 1995.
[15] J. Morlet, G. Arens, I. Fongeau, and P. Giard, "Wave propagation and sampling theory, " *Geophys.*, vol. 47, pp. 203–236, 1982.
[16] A. Grossmann, "Wavelet transforms and edge detection," Ph. Blanchard *et al*., Eds., *Stochastic Processes in Physics and Engineering*. Dordrecht, The Netherlands: Reidel, 1988, pp. 149–157.
[17] N. V. Thakor, J. G. Webster, and W. J. Tompkins, "Estimation of QRS complex power spectra for design of a QRS filter," *IEEE Trans. Biomed. Eng.*, vol. BME-31, pp. 702–706, Nov. 1984.
[18] M. Okada, "A digital filter for the QRS complex detection," *IEEE Trans. Biomed. Eng.*, vol. BME-26, pp. 700–703, Dec. 1979.
[19] S. Suppappola, Y. Sun, and T. A. Wrublewski, "Microcontroller-based real-time QRS detection," *Biomed. Inst. Tech.*, vol. 26, no. 6, pp. 477–484, 1992.
[20] P. S. Hamilton and W. J. Tompkins, "Quantitative investigation of QRS detection rules using the MIT/BIH arrhythmia database," *IEEE Trans. Biomed. Eng.*, vol. BME-33, pp. 1157–1165, 1986.
[21] J. Pan and W. J. Tompkins, "A real-time QRS detection algorithm," *IEEE Trans. Biomed. Eng.*, vol. BME-32, pp. 220–236, Mar. 1985.
[22] R. Murray, "Performance of D_yWT QRS detector on the AHA database," Univ. Rhode Island, Kingston, RI, Tech. Rep. 0994-0001, 1994.
[23] B. Bradie, "Wavelet packet-based compression of single lead ECG," *IEEE Trans. Biomed. Eng.*, vol. 43, pp. 493–501, May 1996.
[24] O. Meste, H. Rix and P. Caminal, and N. V. Thakor, "Ventricular late potentials characterization in time-frequency domain by means of a wavelet transform," *IEEE Trans. Biomed. Eng.*, vol. 41, pp. 625–634, July 1994.
[25] A. Tuzman, M. Acosta, R. Bartesaghi, and T. Hobbins, "Wavelet-based compression of Holter ECG signals," in *Proc. Annu. Int. Conf. IEEE EMBS*, vol. 18, 1996.
[26] S. Papadimitriou, D. Gatzounas, V. Papadopoulos, V. Tzigounis, and A. Bezerianos, "Fetal heart rate signal denoising by processing the wavelet transform modulus maxima," in *Proc. Annu. Int. Conf. IEEE EMBS*, vol. 18, 1996.
[27] D. Ye and X. Ouyang, "Application of wavelet analysis in detection of fetal ECG," in *Proc. Annu. Int. Conf. IEEE EMBS*, vol. 18, 1996.
[28] N. V. Thakor, G. X. Rong, S. Y. Chun, and D. F. Hanley, "Multiresolution wavelet analysis of evoked potentials," *IEEE Trans. Biomed. Eng.*, vol. 40, pp. 1085–1094, Nov. 1993.

Shubha Kadambe (S'85–M'90) received the undergraduate degrees in physics and electronics from Mysore University and Madras institute of Technology, India, in 1977 and 1980, respectively. She received the Ph.D. degree in electrical engineering from the University of Rhode Island, Kingston, in 1991.

From 1980 to 1981, she was a Trainee at Bhabha Atomic research center, a premier research organization in India. She was a Scientific Officer at the same organization from 1981 to 1984. She was a Post-Doctoral Research Fellow at the Applied Science and Engineering Labs, A. I. duPont Institute, Wilmington, DE, from October 1990 to August 1992. During this period, she conducted research in developing speech aids for the handicapped. She was with the Linguistics research department of AT&T Bell Laboratories from September 1992 to December 1994. She conducted research in the areas of language identification and speech recognition while at Bell laboratories. From January 1995 to July 1998, she was with Atlatic Aerospace Electronics Corporation, Greenbelt, MD, where she conducted research in the general areas of time-frequency/time-scale and their applications to speech, sonar and radar, and communications. Since August 1998, she is with HRL Laboratories, Malibu, CA, conducting research in robust and advanced signal processing. She was a Visiting Assistant Professor at the University of Maryland Baltimore County, Baltimore, where she taught graduate courses and served in masters and Ph.D. thesis committees. She is now an Adjunct Assistant Professor at the same university. She has published over 40 journal and conference papers and recently, she has been selected by Marquis to include her biography in their publication of *Who's Who in America*. Her research interests include time-frequency/time-scale and their applications to speech, sonar and radar, speech, neural networks, image processing and nonlinear signal processing.

Dr. Kadambe serves as an Associate Editor of IEEE TRANSACTIONS ON SIGNAL PROCESSING.

Robin Murray, photograph and biography not available at time of publication.

G. Faye Boudreaux-Bartels, photograph and biography not available at time of publication.